On depolarization-evoked exocytosis as a function of calcium entry: possibilities and pitfalls.

Pedersen, Morten Gram

Published in:
Biophysical Journal

DOI:
10.1016/j.bpj.2011.06.061

2011

On depolarization-evoked exocytosis as a function of calcium entry: possibilities and pitfalls

Morten Gram Pedersen[1]
Lund University Diabetes Centre,
Department of Clinical Sciences,
Lund University, Sweden

[1]Lund University Diabetes Centre, Department of Clinical Sciences, Clinical Research Centre, Lund University, CRC 91-11, UMAS entrance 72, SE-20502 Malmö, Sweden. E-mail: morten_gram.pedersen@med.lu.se

Abstract

Secretion from many endocrine cells is a result of calcium-regulated exocytosis due to Ca^{2+}-influx. Using the patch-clamp technique, voltage pulses can be applied to the cells to open Ca^{2+}-channels, resulting in a measurable Ca^{2+}-current, and evoke exocytosis, which can be seen as an increase in membrane capacitance. A common tool for evaluating the relation between Ca^{2+}-influx and exocytosis is to plot the increase in capacitance (ΔC_m) as a function of the integral of the measured Ca^{2+}-current (Q). When depolarizations of different lengths are imposed, the rate of exocytosis is typically higher for shorter than for longer pulses, which has been suggested to result from depletion of a granule pool or from Ca^{2+}-current inactivation. It is here demonstrated that ΔC_m as a function of Q can reveal if Ca^{2+}-current inactivation masquerades as pool depletion. Moreover, it is shown that a convex, cooperativity-like, relation between ΔC_m and Q surprisingly can not occur as a result of cooperative effects, but can result from delays in the exocytotic process or in Ca^{2+}-dynamics. An overview of expected ΔC_m-versus-Q relations for a range of explicit situations is given, which should help in the interpretation of data of depolarization-evoked exocytosis in endocrine cells.

Running title: Exocytosis and calcium entry

Keywords: Large dense-core vesicles, Secretory granules, Exocytosis, Calcium channels, Pool depletion, Capacitance increase

Introduction

Secretion from a variety of endocrine cells is a result of calcium-regulated exocytosis, triggered by Ca^{2+} entry through voltage-gated channels in response to depolarizations (1). The same processes underlie secretion of neurotransmitters, but synaptic release is orders of magnitude faster, and in the following the focus will be on endocrine cells, in particular chromaffin cells and pancreatic β-cells.

The patch-clamp technique has been widely used to investigate the kinetics and Ca^{2+}-sensitivity of exocytosis. Since membrane capacitance is proportional to the area of the membrane, the insertion of granules in the plasma membrane leads to an increase in capacitance that can be measured experimentally (2). Flash-release of 'caged' Ca^{2+} leads to uniform increases in cytosolic Ca^{2+} concentration, which allow direct monitoring of the exocytotic response and its sensitivity to Ca^{2+} (3–8). In voltage-clamp mode, depolarizing pulses can be applied to trigger exocytosis in a more physiological way, because membrane fusion is a result of Ca^{2+}-currents, which can be monitored during the depolarization. However, the membrane capacitance can not be measured during the depolarization for technical reasons, which means that only the total increase in capacitance is obtained (2, 9–11).

To circumvent this limitation of the method one can apply depolarizations of different lengths to approximate the exocytotic response of a hypothetical single capacitance curve (5, 10–17). Typically, the rate of exocytosis is higher for shorter than for longer pulses, which has been suggested to result mainly from depletion of an immediately releasable pool of granules (5, 11) or from Ca^{2+}-current inactivation (10, 12). When Ca^{2+} enters through membrane channels steep spatial gradients are formed creating so-called nanodomains (NDs), where the Ca^{2+}-concentration reaches tens of μM (18). ND-controlled exocytosis is determined mostly by the number of open Ca^{2+}-channels, which can decrease during depolarizations because of channel inactivation. However, in the presence of clusters of Ca^{2+}-channels, the relation is less straight-forward (19).

Another approach to study the exocytotic response to changes in Ca^{2+}-currents is to vary the extra-cellular Ca^{2+}-concentration, which modifies the single-channel current and the ND Ca^{2+}-concentration $[Ca^{2+}]_{ND}$ (5, 12). In this way, the dependence on $[Ca^{2+}]_{ND}$ can be studied more directly, though care must be taken to compensate for screening effects, which shift the activation curve of Ca^{2+}-channels to more positive potentials (20), and faster Ca^{2+}-dependent inactivation (5). Alternatively, the voltage of the depolarizations can be changed (9, 10, 12, 14). These approaches modify both the

number of open channels and the single-channel current, which complicates the data analysis. Naturally, these two approaches can be applied simultaneously or combined with the pulse-length protocol.

A widely used tool for evaluating the relation between Ca^{2+}-influx and exocytosis is to plot the increase in capacitance as a function of the charge, i.e., the integral of the measured Ca^{2+}-current (5, 12, 14, 17). This analysis, while simple to perform, is not completely transparent because of nonlinear dependencies of exocytosis on Ca^{2+}-concentrations, spatial Ca^{2+}-gradients and involvement of various Ca^{2+}-channel types that might couple differently to exocytosis, to name a few possible caveats. The aim of the present manuscript is to provide a deeper analysis of the relation between cumulative capacitance and Ca^{2+} entry resulting from voltage-clamp depolarizations in endocrine cells under a range of explicit assumptions.

A convex or sigmoidal relation between a response variable (e.g., rate of exocytosis) and a triggering variable (e.g. $[Ca^{2+}]$) is the hallmark of cooperativity, and suggests the involvement of >1 unit of the causing variable (e.g., Ca^{2+} ions) in evoking the response (21, 22). Flash-release of caged-Ca^{2+} has established that exocytosis depends cooperatively on the Ca^{2+}-concentration (3–5). This approach investigates the biochemical cooperativity, i.e., the number of Ca^{2+}-ions that needs to bind to a Ca^{2+}-sensor to trigger exocytosis. Current cooperativity considers the rate of exocytosis as a function of the Ca^{2+}-current, and is different from the biochemical cooperativity (23). Channel cooperativity or saturation will here denote, respectively, whether the opening of more channels in a Ca^{2+}-channel cluster increases the probability of exocytosis supra- or sub-linearly. This usage is different from Matveev et al. (23), who used the term channel cooperativity to describe the average number of Ca^{2+}-channels involved in the release of a single vesicle. Finally, a convex or sigmoidal relation between total capacitance increase and Ca^{2+}-entry has been suggested to arise from cooperativity (14, 15, 24). As the present work will show, this is not necessarily the case. Therefore the term cooperativity-like will be used if the total capacitance increase is a convex or sigmoidal function of Ca^{2+}-entry.

Modeling and Results

Mathematical models of biological systems can be classified into two different groups, depending on their purpose (25). "Models-to-simulate" describe the biology based on biophysical, mechanistic hypotheses. Parameter values are usually taken from the literature, or chosen to get reasonable behav-

ior of the model. This type of models has been used also in the study of exocytosis (26, 27). The other approach is to use "models-to-measure" to extract otherwise unknown information, for example from exocytosis data (16, 28). Such models are based on a simpler physiological description of the system under investigation, and the model complexity is minimal to assure more transparent conclusions. This latter modeling approach is used in the following.

Exocytosis is assumed to be triggered from a finite pool of granules (measured in fF) by Ca^{2+} located either in nanodomains below Ca^{2+}-channels or from a general submembrane compartment. The pool size R is described by

$$\frac{dR}{dt} = -E(t)R, \qquad R(0) = R_0, \tag{1}$$

where $E(t)$ is the rate of exocytosis, which is to be specified according to the scenario studied. $E(t)$ will depend on the time-varying Ca^{2+} currents, but is assumed not to depend on $R(t)$. Since refilling of the pool is slow (16, 17, 29, 30), it is assumed not to take place during the short ($<$1 second) depolarizations studied here.

The cumulative capacitance increase during a depolarization ΔC_m reflects the amount of exocytosis and is given by

$$\Delta C_m(t) = R_0 - R(t), \tag{2}$$

since no refilling is assumed. It is also assumed that endocytosis is negligible (31, 32).

Eq. 1 describing the granule pool dynamics can be solved explicitly to yield

$$R(t) = R_0 \exp\left(-\int_0^t E(s)ds\right). \tag{3}$$

When inserting this expression in Eq. 2, the following explicit formula for the cumulative capacitance is obtained,

$$\Delta C_m(t) = R_0\left(1 - \exp\big(-\int_0^t E(u)du\big)\right). \tag{4}$$

The total amount of Ca^{2+} entering during a depolarization of duration t is described by the charge $Q(t) = \int_0^t I_{Ca}(s)ds$, i.e., the integral of the whole cell Ca^{2+}-current I_{Ca}. Through out the manuscript currents and charges are assumed positive, in particular I_{Ca} denotes the absolute value of the calcium current, which by convention is negative when Ca^{2+} flows into the cell.

Pulse-length protocol

A commonly used protocol to study pool depletion is to apply depolarizing pulses of different lengths (10–14). Since capacitance can not be measured reliably during a depolarization, this approach is taken to probe the exocytotic response to a hypothetical single depolarization at several points assuming that the kinetics and pool size does not vary from pulse to pulse. The following subsections analyze the expected relation between cumulative capacitance increase ΔC_m and Ca^{2+}-entry Q under various assumptions.

One Ca^{2+}-channel type, one channel per nanodomain

When granules are located in Ca^{2+}-nanodomains at the inner mouth of Ca^{2+}-channels, the rate of exocytosis is controlled by the nanodomain (ND) Ca^{2+}-concentration, $[Ca^{2+}]_{ND}$. Assume for now that all Ca^{2+}-channels are identical and spatially discrete. Then $[Ca^{2+}]_{ND}$ below an open Ca^{2+}-channel is approximately proportional to the single-channel current i_{Ca} (33). During depolarizations, the whole-cell Ca^{2+}-current I_{Ca} might inactivate, which is caused by the closure of single Ca^{2+}-channels, i.e, the number of open channels decrease during the depolarization but with no change to the single-channel current i_{Ca} through the remaining open channels. This in turn implies that the number of NDs $N_{ND}(t)$, which is proportional to $I_{Ca}(t)$, decreases, but the Ca^{2+}-concentration is unchanged in the remaining NDs. The rate of exocytosis from each ND, $e_{ND} = e_{ND}([Ca^{2+}]_{ND})$, is therefore constant until the collapse of the ND because of closure of the corresponding Ca^{2+}-channel, independently of the functional form of the relation between $[Ca^{2+}]_{ND}$ and e_{ND}. The total rate of exocytosis can then be expressed as

$$E(t) = e_{ND} N_{ND}(t) = e_{ND} I_{Ca}(t)/i_{Ca} = A I_{Ca}(t), \tag{5}$$

where $A = e_{ND}/i_{Ca}$. From Eq. 4 we then obtain

$$\Delta C_m(t) = R_0 \left[1 - \exp\big(-AQ(t)\big)\right]. \tag{6}$$

Note that Eq. 6 describes simple first-order pool kinetics when time is rescaled to $Q(t)$.

If $AQ(t)$ is small, i.e., if the cumulative exocytotic rate is sufficiently low, then the granule pool does not deplete substantially and Eq. 6 simplifies to

$$\Delta C_m(t) = R_0 A Q(t). \tag{7}$$

Thus, in the case of no pool depletion and with exocytosis of each granule controlled by a single channel, cumulative exocytosis is linearly related to

total Ca^{2+} entry (19). However, if the granule pool is eventually depleted, then ΔC_m will be a concave function of Q (Fig. 1A). Hence, ΔC_m must be analyzed as a function of Q to decide whether pool depletion occurs, since Ca^{2+}-channel inactivation might masquerade as pool depletion when considering capacitance increase as a function of depolarization length.

Delayed exocytosis

Flash-release experiments have shown that exocytosis is slightly delayed with respect to a raise in the calcium concentration (5, 13, 16). The analysis of the previous section of the situation with one Ca^{2+}-channel type and one channel and granule per ND carries over with minor changes when a delay is included. Consider a discrete delay τ between the time when Ca^{2+} reaches triggering concentrations in a ND and the formation of the fusion pore that can be seen as an increase in membrane capacitance. The exocytotic rate is now related to the calcium current as

$$E(t) = AI(t-\tau), \tag{8}$$

so that $\Delta C_m = 0$ for $t \leq \tau$ and

$$\Delta C_m(t) = R_0 \left[1 - \exp\big(-AQ(t-\tau)\big)\right], \quad \text{for } t > \tau. \tag{9}$$

The consequence is that $(Q(t), \Delta C_m(t))$ follows the Q-axis until $(Q(\tau), 0)$, before moving upwards. The shape of the curve after the threshold will reflect the relation between ΔC_m and $Q(t-\tau)$ so that in the absence of pool depletion, an almost straight line will be followed, while an near-exponential relation will appear when the pool empties (Fig. 1B, the exact form depends on the shape of I_{Ca}). Considering measurement errors and cell-to-cell variability, the overall relation between Q and ΔC_m might look convex or sigmoidal, deceptively suggesting cooperativity at a first glance.

More realistically, the exocytotic response will have a distributed delay, for example because of a series of steps (a linear chain) before pore formation (4), or subpools with different response times. Then ΔC_m as a function of Q will be a sum of curves leaving the Q-axis at different $Q(\tau_i)$ values (dotted in Fig. 1C), i.e., a sum of curves with the form shown in Fig. 1B. This will result in a smoother departure from the Q-axis, yielding a more cooperativity-like curve, even in the complete absence of cooperativity (Fig. 1C).

Deceptive curvature of ΔC_m as a function of Q

Before considering cases with cooperativity or saturation, a more general result is presented. Assume that E is described as a function of I_{Ca}. The

relation between E and I_{Ca} will be translated below to a description of ΔC_m as a function of Q.

During a depolarization, $(Q(t), \Delta C_m(t))$ describes a plane curve starting at the origin $(0,0)$. Consider a small time step from t to $t+dt$ during which the point $(Q(t), \Delta C_m(t))$ moves to $(Q(t+dt), \Delta C_m(t+dt))$. The direction of this movement is (Fig. 2C)

$$\begin{aligned}\big(Q(t+dt), \Delta C_m(t+dt)\big) - \big(Q(t), \Delta C_m(t)\big) \\ \approx \big(I_{Ca}(t)dt, E(t)R(t)dt\big),\end{aligned} \tag{10}$$

hence, the slope of $(Q(t), \Delta C_m(t))$, i.e, $\frac{d\Delta C_m}{dQ}(t)$, is given by

$$\frac{E(t)R(t)}{I_{Ca}(t)}. \tag{11}$$

If $E(t)$ is a convex function of $I_{Ca}(t)$ (current cooperativity, Fig. 2A, full curve), then $E(t)$ decreases faster than $I_{Ca}(t)$ during inactivation (Fig. 2B). Therefore, $\frac{d\Delta C_m}{dQ}(t)$ will decrease with time, compare open and closed circles in Fig. 2 (representing early and late time-points, respectively). For example, if E is proportional to $[I_{Ca}(t)]^K$, then $\frac{d\Delta C_m}{dQ}(t)$ is proportional to $[I_{Ca}(t)]^{K-1}R(t)$, which decreases over time. Since $Q(t)$ increases over time this implies that ΔC_m is a concave function of Q (Fig. 2C, full curve). This is the case independently of whether pool depletion takes place, though pool depletion would accentuate the decrease in $\frac{d\Delta C_m}{dQ}(t)$ over time. Thus current cooperativity yields a non-obvious relation between Q and ΔC_m, which at first glance could misleadingly suggest saturation or pool depletion. In other words, in the presence of current cooperativity, inactivation of I_{Ca} can masquerade as pool depletion even when ΔC_m is analyzed as a function of Q.

Assuming that the pool size R does not change notably during a depolarization, the opposite is also true. If E is a concave function of I_{Ca}, as in the case of current saturation (Fig. 2B, dashed curve), then ΔC_m is a convex function of Q (Fig. 2C, dashed curve), deceptively giving the suggestion of cooperativity. With pool depletion, sigmoidal $(Q, \Delta C_m)$-curves can be expected, with a convex first part, which then inflects and becomes concave as the pool depletes.

One Ca^{2+}-channel type, more than one channel per nanodomain (channel clustering or domain overlap)

Assume that a cluster of a certain type of Ca^{2+}-channels contain K channels. For example, Barg et al. (5) found that in mouse pancreatic β-cells L-type

Ca^{2+}-channels, the channel type controlling fast exocytosis in these cells (5, 34, 35), are located in clusters of $K \approx 3$ channels. The probability of k of these K channels to be open is (23)

$$P(n = k, t) = \binom{K}{k} p(t)^k (1 - p(t))^{K-k}, \tag{12}$$

where n is a random variable denoting the number of open channels in a cluster, and $p(t)$ is the probability of each channel to be open at time t.

The whole-cell rate of exocytosis is then (23)

$$E(t) = e_{\max} M \sum_{k=1}^{K} r_k \, P(n = k, t), \quad 0 \le r_1 \le \cdots \le r_K = 1, \tag{13}$$

where r_k gives the relative reduction of exocytosis from a ND due to only k of the K channels being open, $e_{\max}$ is the maximal rate of ND-exocytosis, which occurs when all K channels associated with the ND are open, and M is the number of Ca^{2+}-channel clusters.

Two extreme cases can be considered. One can envision that ND-exocytosis is saturated already with one channel open, $r_1 = 1$, meaning that extra Ca^{2+}-influx through other channels does not enhance the probability that a ND-located granule will undergo exocytosis any further. In this case when maximal exocytosis is obtained with at least one open channel, Eq. 13 becomes

$$E(t) = e_{\max} M \left(1 - (1 - p(t))^K\right). \tag{14}$$

As shown in Fig. 2B (dashed curve) for $K = 5$, this relation is concave as expected for a saturation curve. Since p is proportional to I_{Ca}, the same holds for E as a function of I_{Ca}. However, the result from the previous section yields that ΔC_m is a *convex* function of Q, which could deceptively suggest cooperativity (Fig. 2C, dashed curve).

At the other extreme, consider the case when all channels need to be open to trigger exocytosis, i.e., $r_{K-1} = 0$. Then

$$E(t) = e_{\max} M p(t)^K, \tag{15}$$

which is a convex relation. This implies that E is a convex function of I_{Ca} in this case of extreme channel cooperativity (Fig. 2B, full curve), but using the result from the previous section, that ΔC_m is a *concave* function of Q, misleadingly suggesting saturation (Fig. 2C, full curve).

Note that in practice the dependence of exocytosis on the number of open Ca^{2+}-channels in a cluster will be somewhere between the two extremes considered above, and the resulting relation between Q and ΔC_m will describe

a curve lying between the dashed and solid curves in Fig. 2C. Considering cell-to-cell variation and measurement errors, this curve will therefore often appear near-linear in the absence of pool depletion. Thus, channel clustering can not be expected to change the conclusions from the single-channel ND case greatly: only a clear concave deviation from a linear relation between Q and ΔC_m suggests pool depletion.

Several Ca^{2+}-channel types

Endocrine cells express several types of Ca^{2+}-channels (14, 34, 36, 37). When exocytosis is controlled from NDs below one type of Ca^{2+}-channels, e.g. L-type Ca^{2+}-channels in mouse β-cells (5, 34, 35), but not from NDs arising from other types of Ca^{2+}-currents, then the analysis is complicated by the fact that these other channels (e.g., non-L-type in mouse β-cells) contribute to Ca^{2+} entry, Q, but not to cumulative exocytosis, ΔC_m.

Assume for notational simplicity that exocytosis is controlled by L-type Ca^{2+}-channels, but not by non-L-type, as in mouse β-cells, and that channels do not form clusters. The analysis performed above for one channel type and no clustering yielding Eq. 6 is still valid when restricted to the charge entering through L-type channels Q_L, and we have

$$\Delta C_m(t) = R_0 \left[1 - \exp\left(- A_L Q_L(t)\right)\right]. \tag{16}$$

If L-type and non-L-type channels have similar inactivation kinetics, then Q_L and Q are approximately proportional, and Eq. 16 yields readily that Eq. 6 still holds. This scenario covers also the case where some, but not all, L-type Ca^{2+}-channels are associated with a granule, if one assumes that granule-binding does not affect the kinetics of inactivation.

When non-L-type Ca^{2+}-channels have inactivation kinetics different from L-type channels (Supplementary Fig. S1A), the situation is more complex. Consider first that the non-L-type current inactivates much more slowly than the L-type current. Then for longer depolarizations Q will increase faster than Q_L and ΔC_m, resulting in a saturation of ΔC_m as a function of Q, even in the case of no pool depletion and a linear relation between ΔC_m and Q_L (Fig. S1B).

The opposite is also true. If non-L-type channels inactivate rapidly, then for short depolarizations non-L-type channels contribute to Q, giving a shallow slope of ΔC_m as a function of Q, while for longer depolarizations and higher values of Q there is little contribution from non-L-type currents. Thus, at the end of long depolarizations Q and Q_L grow in parallel, and in the absence of pool depletion ΔC_m approaches a linear function of Q, but

with steeper slope than at low Q-values. When pool depletion is substantial ΔC_m will approach an exponential function of Q. The overall relation between ΔC_m and Q can therefore look either convex or sigmoidal, even with no cooperativity assumed (Fig. S1C). However, the deviation from the single-channel relation between ΔC_m and Q is less pronounced in this case than for slowly inactivating non-L-type channels, since the relation will resemble the single-channel curve once the non-L-type current is inactivated, meaning that only the first part of the curve will be strictly convex.

Exocytosis from a submembrane Ca^{2+}compartment

If exocytosis occurs away from Ca^{2+} channels from a more general Ca^{2+} submembrane compartment, and not from Ca^{2+} NDs, then exocytosis will be delayed compared to I_{Ca} because of the time required for diffusion from the Ca^{2+}-channels to the Ca^{2+}-sensor of the exocytotic machinery, even though the submembrane Ca^{2+} concentration $[Ca^{2+}]_{\mathrm{mem}}$ experienced by the granules is lower than the ND concentrations (18). The time-dependence of exocytosis is in this case caused by the dynamics of $[Ca^{2+}]_{\mathrm{mem}}$ and the inactivation of the whole-cell Ca^{2+}-current I_{Ca} rather than the collapse of single NDs. For this reason, no distinction between Ca^{2+}-channel types is required.

A simple model capturing these mechanisms can be formulated as follows. Ca^{2+} flows into the submembrane compartment and is removed, e.g., by pumps, diffusion to the interior of the cell or other means, with the flux assumed linearly related to $[Ca^{2+}]_{\mathrm{mem}}$ (38). It is assumed that buffering of Ca^{2+} occurs rapidly compared to the change in $[Ca^{2+}]_{\mathrm{mem}}$, i.e., the rapid buffer approximation holds (18, 38). This leads to

$$\frac{dCa}{dt} = f(\alpha I_{Ca}(t) - k(Ca - Ca_c)), \qquad Ca(0) = Ca_c, \tag{17}$$

where Ca denotes $[Ca^{2+}]_{\mathrm{mem}}$, f is the fraction of free to total Ca^{2+}, α changes current to flux, k is the rate constant of Ca^{2+} removal and diffusion into the cell, and Ca_c is background, cytosolic Ca^{2+}, and is assumed constant because of the short durations of the depolarizations.

The rate of exocytosis estimated from flash-release of caged-Ca^{2+} is typically a sigmoidal function of the Ca^{2+} concentration reflecting the biochemical cooperativity (3–5, 8), and is therefore modeled as (27)

$$E(Ca) = \frac{E_{\max} Ca^n}{K_E^n + Ca^n}, \tag{18}$$

where $E_{\max}$ is the maximal exocytotic rate, n is the Hill-coefficient measuring the biochemical Ca^{2+}-cooperativity, and K_E the $[Ca^{2+}]_{\text{mem}}$ giving half-maximal rate.

Solving Eq. 17 yields the explicit expression

$$Ca(t) = Ca_c + f\alpha \int_0^t I_{Ca}(s) \exp[-fk(t-s)]ds, \tag{19}$$

i.e., Ca responds to I_{Ca} after a distributed delay. Combining this observation with Eq. 18 means that exocytosis responds to I_{Ca} after a (distributed) delay, which suggests that some of the findings concerning ΔC_m versus Q from the section investigating explicit delays in the exocytotic process might be applicable here as well, in particular that a cooperativity-like relation could appear.

From Eq. 11 it is seen that the slope of $(Q(t), \Delta C_m(t))$ is given by $E(Ca(t))R(t)/I_{Ca}(t)$, and since $I_{Ca}(t)$ decreases over time due to inactivation (Fig. 3A), while $Ca(t)$ and hence $E(Ca)$ increases at the beginning of depolarizations (Fig. 3B), the slope will increase with time. Thus, ΔC_m will have a cooperativity-like relation to Q, mainly because of the delay in exocytosis caused by the slow build-up of $[Ca^{2+}]_{\text{mem}}$. Interestingly, the upward curvature is typically accentuated by the fact that $[Ca^{2+}]_{\text{mem}}$ is low at the beginning of a depolarization, so that $E(Ca)$ is on the convex part of the sigmoidal curve (Fig. 3C) and is approximately proportional to Ca^n. It might be expected from the analysis in the previous sections that the cooperative dependence of E on Ca would result in a concave relation between ΔC_m and Q, counteracting the convexity caused by the slow increase in $[Ca^{2+}]_{\text{mem}}$. However, this slower $[Ca^{2+}]_{\text{mem}}$ response changes the decreasing I_{Ca}-trace to an increasing $[Ca^{2+}]_{\text{mem}}$-curve (39) (Fig. 3AB), and therefore ΔC_m as a function of Q inherits the curvature from $E(Ca)$ on the early part of the curve, accentuating the cooperativity-like relation due to the slow $[Ca^{2+}]_{\text{mem}}$ build-up (Fig. 3D).

After fast transients in I_{Ca}, Ca approaches a quasi-steady level given by $Ca_* = \alpha I_{Ca}(t)/k + Ca_c$. This means that exocytosis continues with a quasi-steady rate $E(Ca_*)$ so that ΔC_m increases near-linearly in the absence of pool depletion. Also Q increases near-linearly, since I_{Ca} is now approximately constant, and hence, ΔC_m approaches a linear function of Q at the end of longer depolarizations. This will be the case independently of the magnitude of Ca_* compared to K_E, and hence no hint of the calcium sensitivity can be obtained from the pulse-length protocol, in particular plotting ΔC_m as function of Q will not reveal if the exocytotic rate is saturated as a function of $[Ca^{2+}]_{\text{mem}}$(Fig. 3CD). Thus, the overall relation between ΔC_m

and Q will appear cooperativity-like since the first part of the curve will bend upwards while Ca increases and I_{Ca} inactivates, while the later part of the curve will be approximately linear when the quasi-steady state is reached (Fig. 3D). The curvature of the convex curve will have no direct relation to the biochemical cooperativity, and if the build-up of $[Ca^{2+}]_{mem}$ is sufficiently rapid, then it might be approximately linear, even in the case of high biochemical cooperativity (12, 40). In the case of pool depletion, the latter part of the curve will become concave as the pool empties.

Varying the external Ca^{2+} concentration or the test potential

An indirect way of studying the biochemical Ca^{2+}-sensitivity and cooperativity of exocytosis using voltage-pulses is to vary the external Ca^{2+} concentration $[Ca^{2+}]_e$, classically done by applying depolarizations of fixed duration (11, 12, 22). Raising $[Ca^{2+}]_e$ will increase single channel Ca^{2+}-currents and ND Ca^{2+}-concentrations below open Ca^{2+}-channels, giving an indirect measure of how exocytosis depends on $[Ca^{2+}]_{ND}$. However, high $[Ca^{2+}]_{ND}$ will in turn accelerate Ca^{2+}-dependent inactivation (5, 33). Thus, the relation between ΔC_m and Q following longer depolarizations is not clear due to competing effects. Moreover, the activation curve of the Ca^{2+}-channels can be shifted to higher potentials due to screening effects (20), and the magnitude of single-channel Ca^{2+}-currents can be a non-linear function of $[Ca^{2+}]_e$ (41), making it difficult to relate $[Ca^{2+}]_e$ to $[Ca^{2+}]_{ND}$.

Assume for simplicity that all Ca^{2+}-channels have identical kinetics, that exocytosis occurs from NDs below single channels, and that pool depletion is negligible. Raised $[Ca^{2+}]_{ND}$ will increase e_{ND} in Eq. 5 unless $[Ca^{2+}]_{ND}$ was already at saturating levels. On the other hand, the single channel current i_{Ca} will also increase, and the relative magnitude of these two increases will determine whether $A = e_{ND}/i_{Ca}$ increases or decreases. The slope between ΔC_m and Q obtained from a pulse-length protocol can be used to estimate A, see Eq. 7. Since $[Ca^{2+}]_{ND}$ is approximately proportional to i_{Ca} (33), an increase in A reflects a cooperative dependence of e_{ND} on $[Ca^{2+}]_{ND}$, while a decrease in A corresponds to e_{ND} being saturated.

For the protocol varying $[Ca^{2+}]_e$, but with fixed depolarization length, the relation between ΔC_m and Q depends also on how Q varies with $[Ca^{2+}]_e$. Each depolarization gives a single point on a pulse-length $(Q, \Delta C_m)$-curve (Fig. S2). If Q increases with $[Ca^{2+}]_e$, meaning that the effect of $[Ca^{2+}]_e$ on i_{Ca} is stronger than screening effects and the effect on Ca^{2+}-current inactivation, then an increase in A will give a convex relation between Q and ΔC_m (Fig. S2, blue curve), thus honestly reflecting the cooperative dependence of

exocytosis (e_{ND}) on $[Ca^{2+}]_{ND}$ (i_{Ca}). However, the coefficient from a polynomial fit is in general unrelated to the intrinsic biochemical cooperativity coefficient.

If A increases but Q decreases when $[Ca^{2+}]_e$ is raised, as seen in pancreatic β-cells for longer depolarizations (5), then the relation between ΔC_m and Q will be concave (Fig. S2, red curve), or might even be decreasing, since little Ca^{2+}-influx (at high $[Ca^{2+}]_e$) could result in more exocytosis than seen with more charge entry at lower $[Ca^{2+}]_e$(Fig. S2, black curve). Vice versa for the case when A is inversely related to $[Ca^{2+}]_e$, reflecting saturation of exocytosis.

In the case of Ca^{2+}-channel clustering, the analysis is further complicated by the fact that channel cooperativity (Fig. 2, solid curves) can be changed to channel saturation (Fig. 2, dashed curves) as $[Ca^{2+}]_e$ is raised. Since i_{Ca} is approximately proportional to $[Ca^{2+}]_e$, at least over a range of $[Ca^{2+}]_e$ (41), varying $[Ca^{2+}]_e$ several fold (5, 12) changes the current flowing through a single channel to a similar extent. If only one channel is open, this directly translates to a several fold change of $[Ca^{2+}]_{ND}$. Given the high intrinsic biochemical cooperativity of the exocytotic process, it is plausible that such a large change in $[Ca^{2+}]_{ND}$ can shift the scenario from channel cooperativity, where a single channel is insufficient to trigger exocytosis, to channel saturation, where the single channel current is evoking near-maximal exocytosis. For the pulse-length protocol the analysis of the previous sections yields that this change is seen as a concave relation between Q and ΔC_m in low $[Ca^{2+}]_e$, but a convex relation at high $[Ca^{2+}]_e$ (Fig. 2). For the protocol varying $[Ca^{2+}]_e$, but with a fixed pulse duration, the relation between ΔC_m and Q can then take a large variety of shapes depending on whether A and Q increases with $[Ca^{2+}]_e$, and the amount of channel cooperativity and saturation at the different $[Ca^{2+}]_e$.

Alternatively, the test potential during the depolarization can be varied (9–12, 14). This modifies both the Ca^{2+}-channel activation kinetics, and as for varying $[Ca^{2+}]_e$, the single channel currents, and hence $[Ca^{2+}]_{ND}$ and Ca^{2+}-dependent inactivation. For test potentials giving maximal activation, the discussion above concerning varying $[Ca^{2+}]_e$ still holds. For low test potentials activating few channels, the single channel current will be bigger, leading to faster Ca^{2+}-dependent inactivation and further lowering the number of open channels. Moreover, different Ca^{2+}-channel types activate at different membrane potentials, and if they couple differently to exocytosis, the analysis will be further complicated. These questions will not be pursued further here.

In short, when exocytosis is controlled by $[Ca^{2+}]_{ND}$, little information is

gained from varying $[Ca^{2+}]_e$ or the test potential with a fixed pulse duration, but considerable insight can be obtained by doing a pulse-length protocol at a range of different $[Ca^{2+}]_e$ or test potentials.

If exocytosis is controlled from a submembrane compartment away from Ca^{2+}-channels, then the properties of single channels is unimportant, and only the total current I_{Ca} matters, as seen from Eq. 17. Varying the test potential or $[Ca^{2+}]_e$ will in this case not change the Q versus ΔC_m relation substantially, though larger currents might accelerate the build-up of Ca^{2+}, resulting in a shorter delay between I_{Ca} and exocytosis, which will show up as a slight left shift of ΔC_m as a function of Q in the pulse-length protocol.

Discussion

The voltage-clamp pulse protocols are widely used as a relatively easy and physiological method for investigating the relation between Ca^{2+} and exocytosis. However, it is becoming increasingly evident that the biochemical dependence on Ca^{2+} intrinsic to the exocytotic process is hard to extract from this kind of data (23). This is further illustrated in the present manuscript. Thus, flash-release of caged-Ca^{2+} remains the preferred method for studying directly how Ca^{2+} controls exocytosis. However, flash-release experiments need to be done using the whole-cell configuration, which is known to alter the exocytotic response compared to perforated-patch recordings (42).

One advantage of the voltage-clamp protocol is that it allows the study of different granule pools, in particular the IRP using the pulse-length protocol (5, 11, 13). As widely recognized (11, 12, 17, 30, 40, 43, 44), the exocytotic response ΔC_m must be set in relation to the Ca^{2+}-current, for example to Q, the total amount of Ca^{2+} that entered the cell during the depolarization, to evaluate whether pool depletion occurred, as highlighted in Eqs. 5-7. Thus, if pool depletion is dominant, ΔC_m will be a saturating function of Q. If ΔC_m plateaus for longer pulse durations because of Ca^{2+}-channel inactivation, then the relation between ΔC_m and Q will be linear. This is true for the simplest case where each releasable granule is associated with a single Ca^{2+}-channel and its nanodomain, but might not hold for more complex scenarios, as summarized in Table 1.

Of particular notice is the finding that a clear convex, cooperativity-like, relation between ΔC_m and Q can be caused by delays, either in the exocytotic machinery or in the slow build-up of submembrane Ca^{2+}, but neither channel nor biochemical cooperativity result in a convex $(Q, \Delta C_m)$-curve. In contrast, channel saturation can result in a weakly convex relation (Fig. 2C).

The inverted curvature is caused by inactivation of I_{Ca}, which means that the $(I_{Ca}(t), E(t))$-curve is followed backwards in time, while $(Q(t), \Delta C_m(t))$ is not (Fig. 2). Therefore, the slope of $(Q(t), \Delta C_m(t))$, given by Eq. 11, will at low Q-values reflect the size of E and I_{Ca} at high I_{Ca}-values, and vice versa.

It is also noteworthy that Ca^{2+}-current inactivation can masquerade as pool depletion, not only when plotted as a function of depolarization length, but also when considered as a function of Ca^{2+}-entry, either in the presence of channel cooperativity (Fig. 2C), or more clearly when exocytosis is controlled mainly by a Ca^{2+}-current type with rapid inactivation compared to other Ca^{2+}-channel types with weaker coupling to exocytosis (Fig. S1B). This latter scenario must be considered for example for chromaffin cells located in mouse adrenal slices, which show a concave relation between ΔC_m and Q (17), but where exocytosis is mainly controlled by rapidly inactivating R-type Ca^{2+}-currents (36). Thus, the pulse-length protocol is not optimal for the investigation of depletion of an IRP, and a dual-pulse protocol should be preferred (43). Indeed, the application of this protocol has shown that pool depletion does happen in chromaffin cells located in mouse adrenal slices (16).

The presence of several pools, for example a small IRP located in Ca^{2+}-channel NDs and a HCSP located away from Ca^{2+}-channels (6–8, 16), could show up as more complicated $(Q(t), \Delta C_m(t))$-curves. For example, the depletion of an IRP would give an exponential relation (Eq. 6) for low Q-values, but the recruitment of a submembrane controlled HCSP will give a convex or linear relation for higher Q-values. Depending of the degree of overlap, this could give a near-linear relation or a distinct N-shaped curve, which goes from concave to convex as Q increases.

This example highlights the fact that it is hard to draw clear conclusions from a simple ΔC_m-versus-Q plot, see also Table 1. However, scenarios can be ruled out, for example a convex $(Q(t), \Delta C_m(t))$-curve can not result from cooperativity alone. To further narrow down the possible arrangement and control of granule pools, additional experiments are needed. For example, the use of exogenous buffers can be used to suppress exocytosis away from Ca^{2+}-channels (5, 17, 18), flash-release can investigate inherent delays in the exocytotic process (3–8), or blockage of different Ca^{2+}-channel types can be used to investigate the control by specific channel types (12, 14, 35, 36, 40), and their inactivation kinetics can then be compared to the kinetics of other channel types not directly involved in exocytosis.

Comparing different cell types, it is worth noticing that single mouse β-cells have been found to have a linear relation between Q and ΔC_m in re-

sponse to depolarizations of different durations (5, 45), in agreement with the prediction of the theory presented here if exocytosis is controlled by L-type Ca^{2+}-channel NDs (5, 34, 35) and the IRP does not deplete notably during these depolarizations (Fig. 1, Eq. 7 and Table 1). A linear relationship has also been found in single mouse pancreatic α-cells (37, 44). It should be noted that L-type and non-L-type channels have similar inactivation kinetics in mouse β-cells since L-type channel contribute to $\sim$60 % of both the peak Ca^{2+}-current (46) and the integrated current Q during a 100 ms depolarization (34). In contrast, single human β-cells have Ca^{2+}-channel types with great differences in inactivation kinetics (14). Moreover, exocytosis is evoked only in response to longer depolarizations and ΔC_m is a highly convex function of Q (14, 15), two facts that suggest that granules are located away from Ca^{2+}-channels in these cells. However, flash-release experiments to rule out inherent delays in exocytosis, and depolarizations with high Ca^{2+}-buffer, e.g. EGTA, concentrations are needed to test this hypothesis.

Chromaffin cells show a less clear relation between ΔC_m and Q. There is good evidence for depletion of an IRP in response to short depolarizations using the whole-cell method (6, 11, 16, 17, 43), while the exocytotic response to longer depolarization and in the perforated-patch configuration gives a linear (47) or convex function of Ca^{2+}-entry Q (12). As shown here, such relations could be explained by the release of granules located away from Ca^{2+}-channels (see also (16, 26)). In single mouse chromaffin cells the IRP appears to be lost, and a linear relation between ΔC_m and Q is found in response to the pulse-length protocol (17). In contrast, the IRP is present in mouse chromaffin cells in adrenal slice preparations (16, 17) where it is affected more by BAPTA than by EGTA (17), indicating that it is located in NDs below Ca^{2+}-channels (18). These different findings suggest the presence of a releasable pool located away from Ca^{2+}-channels, such as a HCSP, in addition to the IRP (6, 16, 26). The linear or convex relation between ΔC_m and Q in single chromaffin cells could be due to the overlap of exocytosis from these pools, see above. The results from mouse adrenal slices fits into this picture if a larger IRP and a clearer distinction between pools are assumed. Alternatively the linear dependence of ΔC_m on Q could arise from release of a submembrane-located pool if $[Ca^{2+}]_{\mathrm{mem}}$ responds quickly to I_{Ca}. The fact that a concave relationship is seen also for longer depolarizations in the presence of EGTA (17) supports this picture, since EGTA suppresses exocytosis away from Ca^{2+}-channels, which could allow the depletion of the IRP to appear in the ΔC_m-versus-Q plot.

Finally a short note on the presentation of results from the so-called train protocol. When stimulating the cell with a train of identical pulses, it is typ-

ically found that Ca^{2+}-entry $Q(n)$ and cumulative capacitance $\Delta C_m(n)$ per pulse decreases as a function of pulse number n (5, 13, 15, 30, 48). There are two ways of visualizing the relation between Ca^{2+}-entry Q and cumulative capacitance ΔC_m, either as per pulse results (15) (Fig. S3B), or as cumulative quantities through out the train (48) (Fig. S3C). The curvature of these two curves will be opposite if $Q(n)$ decreases from pulse to pulse, which can be seen as follows. If $\sum_{n=1}^{N} \Delta C_m(n)$ is a concave function of $\sum_{n=1}^{N} Q(n)$ (Fig. S3C), then $\Delta C_m(n)/Q(n)$ decreases with n, and vice versa. Since $Q(n)$ decreases with n, the relation between $\Delta C_m(n)$ and $Q(n)$ will be convex (Fig. S3B). Thus, if a pool of granules depletes (saturation of $\sum_n \Delta C_m(n)$ vs $\sum_n Q(n)$) then, deceivingly, this would appear as a cooperativity-like per-pulse relation between $\Delta C_m(n)$ versus $Q(n)$. The opposite is true when $\Delta C_m(n)/Q(n)$ increases with n. These conclusions are independent of any assumptions on calcium sensitivity or spatial control of exocytosis and refilling.

In summary, care must be taken when interpreting ΔC_m as a function of Q. It is most suitable for the study of exocytosis in response to short depolarizations at different durations. Inactivation of I_{Ca} can masquerade as pool depletion, and the curvature of the relation can misleadingly suggest cooperativity or saturation. In spite of such pitfalls, the relation between ΔC_m and Q from a pulse-length protocol can be useful as a reference, to which one can compare results from disease or mutant animal models, even if the Ca^{2+}-currents are different in the two groups. However, if the relationship is changed, then further studies are needed to understand the underlying cause of this modification of ΔC_m as a function of Q. Valuable insight can be obtained by varying the test potential or $[Ca^{2+}]_e$, but this should be combined with full pulse-length protocols under the various conditions. Knowledge about the kinetics of different Ca^{2+}-channel types and their involvement in exocytosis from experiments with Ca^{2+}-channel antagonists is necessary for a complete picture. In the case when exocytosis is mainly occurring away from Ca^{2+}-channels, the dynamics of $[Ca^{2+}]_{mem}$, which can be modulated by exogenous buffers such as EGTA, is the most important factor in determining the relation between ΔC_m and Q.

Acknowledgments

I wish to thank Dr. Arthur Sherman for careful reading of an earlier version of the manuscript, and Prof. Patrik Rorsman for addressing my attention to the problem.

Grants

This work was supported by the EU through a Marie Curie Intra-European Fellowship.

References

1. Burgoyne, R. D., and A. Morgan, 2003. Secretory granule exocytosis. *Physiol Rev* 83:581–632.

2. Lindau, M., and E. Neher, 1988. Patch-clamp techniques for time-resolved capacitance measurements in single cells. *Pflugers Arch* 411:137–146.

3. Thomas, P., J. G. Wong, A. K. Lee, and W. Almers, 1993. A low affinity Ca2+ receptor controls the final steps in peptide secretion from pituitary melanotrophs. *Neuron* 11:93–104.

4. Heinemann, C., R. H. Chow, E. Neher, and R. S. Zucker, 1994. Kinetics of the secretory response in bovine chromaffin cells following flash photolysis of caged Ca2+. *Biophys J* 67:2546–2557.

5. Barg, S., X. Ma, L. Eliasson, J. Galvanovskis, S. O. Göpel, S. Obermüller, J. Platzer, E. Renström, M. Trus, D. Atlas, J. Striessnig, and P. Rorsman, 2001. Fast exocytosis with few Ca(2+) channels in insulin-secreting mouse pancreatic B cells. *Biophys J* 81:3308–3323.

6. Yang, Y., S. Udayasankar, J. Dunning, P. Chen, and K. D. Gillis, 2002. A highly Ca2+-sensitive pool of vesicles is regulated by protein kinase C in adrenal chromaffin cells. *Proc Natl Acad Sci U S A* 99:17060–17065.

7. Yang, Y., and K. D. Gillis, 2004. A highly Ca2+-sensitive pool of granules is regulated by glucose and protein kinases in insulin-secreting INS-1 cells. *J Gen Physiol* 124:641–651.

8. Wan, Q.-F., Y. Dong, H. Yang, X. Lou, J. Ding, and T. Xu, 2004. Protein kinase activation increases insulin secretion by sensitizing the secretory machinery to Ca2+. *J Gen Physiol* 124:653–662.

9. Thomas, P., A. Surprenant, and W. Almers, 1990. Cytosolic Ca2+, exocytosis, and endocytosis in single melanotrophs of the rat pituitary. *Neuron* 5:723–733.

10. Ammälä, C., L. Eliasson, K. Bokvist, O. Larsson, F. M. Ashcroft, and P. Rorsman, 1993. Exocytosis elicited by action potentials and voltage-clamp calcium currents in individual mouse pancreatic B-cells. *J Physiol* 472:665–688.

11. Horrigan, F. T., and R. J. Bookman, 1994. Releasable pools and the kinetics of exocytosis in adrenal chromaffin cells. *Neuron* 13:1119–1129.

12. Engisch, K. L., and M. C. Nowycky, 1996. Calcium dependence of large dense-cored vesicle exocytosis evoked by calcium influx in bovine adrenal chromaffin cells. *J Neurosci* 16:1359–1369.

13. Barg, S., J. Galvanovskis, S. O. Göpel, P. Rorsman, and L. Eliasson, 2000. Tight coupling between electrical activity and exocytosis in mouse glucagon-secreting alpha-cells. *Diabetes* 49:1500–1510.

14. Braun, M., R. Ramracheya, M. Bengtsson, Q. Zhang, J. Karanauskaite, C. Partridge, P. R. Johnson, and P. Rorsman, 2008. Voltage-gated ion channels in human pancreatic beta-cells: electrophysiological characterization and role in insulin secretion. *Diabetes* 57:1618–1628.

15. Braun, M., R. Ramracheya, P. R. Johnson, and P. Rorsman, 2009. Exocytotic properties of human pancreatic beta-cells. *Ann N Y Acad Sci* 1152:187–193.

16. Voets, T., E. Neher, and T. Moser, 1999. Mechanisms underlying phasic and sustained secretion in chromaffin cells from mouse adrenal slices. *Neuron* 23:607–615.

17. Moser, T., and E. Neher, 1997. Rapid exocytosis in single chromaffin cells recorded from mouse adrenal slices. *J Neurosci* 17:2314–2323.

18. Neher, E., 1998. Vesicle pools and Ca2+ microdomains: new tools for understanding their roles in neurotransmitter release. *Neuron* 20:389–399.

19. Augustine, G. J., E. M. Adler, and M. P. Charlton, 1991. The calcium signal for transmitter secretion from presynaptic nerve terminals. *Ann N Y Acad Sci* 635:365–381.

20. Hille, B., 2001. Ion Channels of Excitable Membranes. Sinauer Associates, Inc., Sunderland, MA, U.S.A., 3rd edition.

21. Weiss, J. N., 1997. The Hill equation revisited: uses and misuses. *FASEB J* 11:835–841.

22. Dodge, F. A., and R. Rahamimoff, 1967. Co-operative action a calcium ions in transmitter release at the neuromuscular junction. *J Physiol* 193:419–432.

23. Matveev, V., R. Bertram, and A. Sherman, 2009. Ca2+ current versus Ca2+ channel cooperativity of exocytosis. *J Neurosci* 29:12196–12209.

24. Brandt, A., D. Khimich, and T. Moser, 2005. Few CaV1.3 channels regulate the exocytosis of a synaptic vesicle at the hair cell ribbon synapse. *J Neurosci* 25:11577–11585.

25. Cobelli, C., C. Dalla Man, G. Sparacino, L. Magni, G. De Nicolao, and B. P. Kovatchev, 2009. Diabetes: Models, Signals, and Control. *IEEE Reviews in Biomedical Engineering* 2:54–96.

26. Klingauf, J., and E. Neher, 1997. Modeling buffered Ca2+ diffusion near the membrane: implications for secretion in neuroendocrine cells. *Biophys J* 72:674–690.

27. Pedersen, M. G., and A. Sherman, 2009. Newcomer insulin secretory granules as a highly calcium-sensitive pool. *Proc Natl Acad Sci U S A* 106:7432–7436.

28. Chow, R. H., J. Klingauf, and E. Neher, 1994. Time course of Ca2+ concentration triggering exocytosis in neuroendocrine cells. *Proc Natl Acad Sci U S A* 91:12765–12769.

29. Gromada, J., M. Høy, E. Renström, K. Bokvist, L. Eliasson, S. Göpel, and P. Rorsman, 1999. CaM kinase II-dependent mobilization of secretory granules underlies acetylcholine-induced stimulation of exocytosis in mouse pancreatic B-cells. *J Physiol* 518:745–759.

30. Rose, T., S. Efendic, and M. Rupnik, 2007. Ca2+-secretion coupling is impaired in diabetic Goto Kakizaki rats. *J Gen Physiol* 129:493–508.

31. Eliasson, L., P. Proks, C. Ammälä, F. M. Ashcroft, K. Bokvist, E. Renström, P. Rorsman, and P. A. Smith, 1996. Endocytosis of secretory granules in mouse pancreatic beta-cells evoked by transient elevation of cytosolic calcium. *J Physiol* 493:755–767.

32. Smith, C., and E. Neher, 1997. Multiple forms of endocytosis in bovine adrenal chromaffin cells. *J Cell Biol* 139:885–894.

33. Sherman, A., J. Keizer, and J. Rinzel, 1990. Domain model for Ca2(+)-inactivation of Ca2+ channels at low channel density. *Biophys J* 58:985–995.

34. Schulla, V., E. Renström, R. Feil, S. Feil, I. Franklin, A. Gjinovci, X.-J. Jing, D. Laux, I. Lundquist, M. A. Magnuson, S. Obermüller, C. S. Olofsson, A. Salehi, A. Wendt, N. Klugbauer, C. B. Wollheim, P. Rorsman, and F. Hofmann, 2003. Impaired insulin secretion and glucose tolerance in beta cell-selective Ca(v)1.2 Ca2+ channel null mice. *EMBO J* 22:3844–3854.

35. Göpel, S., Q. Zhang, L. Eliasson, X.-S. Ma, J. Galvanovskis, T. Kanno, A. Salehi, and P. Rorsman, 2004. Capacitance measurements of exocytosis in mouse pancreatic alpha-, beta- and delta-cells within intact islets of Langerhans. *J Physiol* 556:711–726.

36. Albillos, A., E. Neher, and T. Moser, 2000. R-Type Ca2+ channels are coupled to the rapid component of secretion in mouse adrenal slice chromaffin cells. *J Neurosci* 20:8323–8330.

37. Marinis, Y. Z. D., A. Salehi, C. E. Ward, Q. Zhang, F. Abdulkader, M. Bengtsson, O. Braha, M. Braun, R. Ramracheya, S. Amisten, A. M. Habib, Y. Moritoh, E. Zhang, F. Reimann, A. H. Rosengren, T. Shibasaki, F. Gribble, E. Renström, S. Seino, L. Eliasson, and P. Rorsman, 2010. GLP-1 inhibits and adrenaline stimulates glucagon release by differential modulation of N- and L-type Ca2+ channel-dependent exocytosis. *Cell Metab* 11:543–553.

38. Sherman, A. S., Y.-X. Li, and J. E. Keizer, 2002. Whole-Cell Models. *In* C. P. Fall, E. S. Marland, J. M. Wagner, and J. J. Tyson, editors, Computational Cell Biology. Springer, New York, Chapter 5, 101–139.

39. Hoppa, M. B., S. Collins, R. Ramracheya, L. Hodson, S. Amisten, Q. Zhang, P. Johnson, F. M. Ashcroft, and P. Rorsman, 2009. Chronic palmitate exposure inhibits insulin secretion by dissociation of Ca(2+) channels from secretory granules. *Cell Metab* 10:455–465.

40. Mansvelder, H. D., and K. S. Kits, 2000. All classes of calcium channel couple with equal efficiency to exocytosis in rat melanotropes, inducing linear stimulus-secretion coupling. *J Physiol* 526:327–339.

41. Church, P. J., and E. F. Stanley, 1996. Single L-type calcium channel conductance with physiological levels of calcium in chick ciliary ganglion neurons. *J Physiol* 496:59–68.

42. Augustine, G. J., and E. Neher, 1992. Calcium requirements for secretion in bovine chromaffin cells. *J Physiol* 450:247–71.

43. Gillis, K. D., R. Mossner, and E. Neher, 1996. Protein kinase C enhances exocytosis from chromaffin cells by increasing the size of the readily releasable pool of secretory granules. *Neuron* 16:1209–1220.

44. Andersson, S. A., M. G. Pedersen, J. Vikman, and L. Eliasson, 2011. Glucose-dependent docking and SNARE protein-mediated exocytosis in mouse pancreatic alpha-cell. *Pflugers Arch.* In Press.

45. Vikman, J., X. Ma, G. H. Hockerman, P. Rorsman, and L. Eliasson, 2006. Antibody inhibition of synaptosomal protein of 25 kDa (SNAP-25) and syntaxin 1 reduces rapid exocytosis in insulin-secreting cells. *J Mol Endocrinol* 36:503–515.

46. Vignali, S., V. Leiss, R. Karl, F. Hofmann, and A. Welling, 2006. Characterization of voltage-dependent sodium and calcium channels in mouse pancreatic A- and B-cells. *J Physiol* 572:691–706.

47. Thiagarajan, R., J. Wilhelm, T. Tewolde, Y. Li, M. M. Rich, and K. L. Engisch, 2005. Enhancement of asynchronous and train-evoked exocytosis in bovine adrenal chromaffin cells infected with a replication deficient adenovirus. *J Neurophysiol* 94:3278–3291.

48. Engisch, K. L., N. I. Chernevskaya, and M. C. Nowycky, 1997. Short-term changes in the Ca2+-exocytosis relationship during repetitive pulse protocols in bovine adrenal chromaffin cells. *J Neurosci* 17:9010–9025.

Table

Scenario	Pool depletion:		Figure	Examples:	
	with	without		with	without
Single-channel ND (SCND)	concave	linear	Fig. 1A	(17, 45)	(5, 17, 37, 45, 47)
SCND + delay	sigmoidal	convex	Fig. 1BC		
Cluster, ch.-saturation	*sigmoidal*	*convex*	Fig. 2B		(45)
Cluster, ch.-cooperativity	concave	*concave*	Fig. 2C		
SCND + other fast ch.-type	*sigmoidal*	*convex*	Fig. S1B		
SCND + other slow ch.-type	concave	concave	Fig. S1C	(17)	
Submembrane	sigmoidal	convex	Fig. 3D		(12, 14)

Table 1: Overview of expected relations between ΔC_m and Q in the pulse-length protocol in various scenarios (ch.=channel), with references to the corresponding figures in this work. Italic fonts are used to indicate weak curvatures. Examples from the literature that might correspond to the scenarios with or without pool depletion are suggested in the last two columns.

Figure Captions

Figure 1

Cumulative capacitance ΔC_m as a function of Ca^{2+}-entry Q for the case of single-channel nanodomains controlling exocytosis. Simulations of Eqs. 4-5 with $I_{Ca}(t) = 120$ pA $\exp(-t/100\text{ms})$ (5) with either $R_0 = 50$ fF and $A = 0.2/\text{pC}$ (pool depletion), or $R_0 = 1000$ fF and $A = 0.01/\text{pC}$ (no depletion). A: In the case of no delay, the relation is exponential (dashed curve, Eq. 6), which simplifies to a linear function in the absence of pool depletion (solid curve, Eq. 7). B: With a single, explicit delay (here, $\tau = 15$ ms (5)), the x-axis is followed until $(Q(\tau), 0)$, after which the relation is approximately exponential (dashed, Eq. 9) or linear (solid curve). The grey curves are from panel A. C: With distributed or several delays (here, 5 pools with delays $\tau = 5 - 25$ ms and total size as in panel A were simulated), the overall relation is either sigmoidal (dashed curve) or, in the absence of pool depletion, convex (solid). The dotted curves indicate the progressive sums of single-delay curves (compare with solid, black curve in panel B), corresponding to the progressive release of pools with different delays and no pool depletion. The grey curves are from panel A.

Figure 2

Inverted curvature of ΔC_m as a function of Q illustrated by the special case of channel clustering. A: Exocytosis is assumed to result from nanodomains below channel clusters, either for the case of channel saturation (concave, dashed curve; Eq. 14 with $K = 5$) or for the case of channel cooperativity (convex, solid curve; Eq. 15 with $K = 3$). B: The whole-cell Ca^{2+}-current I_{Ca} is assumed to inactivate with a time-constant of 100 ms (grey curve). Exocytosis as a function of time is shown for the case of channel saturation (dashed curve) and channel cooperativity (black, solid curve) calculated from the functions shown in panel A. C: The curvature of ΔC_m as a function of Q is inverted compared to panel B, and is convex in the in the case of channel saturation (dashed curve), while it is concave with channel cooperativity (solid curve). The open and closed circles indicate the corresponding variables at an early and a later time-point, respectively. See main text for further details. All variables have been normalized for easier comparison.

Figure 3

Cooperativity-like relation between ΔC_m and Q when exocytosis occurs away from Ca^{2+}-channels. Simulation of Eqs. 17-18 with parameters $E_{\max} = 1000$ fF/s, $K_E = 2$ μM, $n = 3$, $f = 0.01$, $\alpha = 50$ μM/s/pA, $k = 300$ s^{-1}, $Ca_c = 0.2$ μM.A: The whole-cell Ca^{2+}-current is assumed to consist of two parts with one sustained component and another component that inactivates exponentially with a time-constant of 100 ms, $I_{Ca} = (0.3{+}0.7\exp[-t/100\text{ms}])\times$ 100 pA. B: The $[Ca^{2+}]_{\text{mem}}$-trace is increasing as a function of time due to its delayed build-up. C: The exocytotic rate E is assumed to be saturated by $[Ca^{2+}]_{\text{mem}}$ for most of the experiment. The circle indicates the inflection point after which saturation occurs. The same point is shown in the other panels. D: Even after E is saturated, ΔC_m as a function of Q follows a convex curve.

Figures

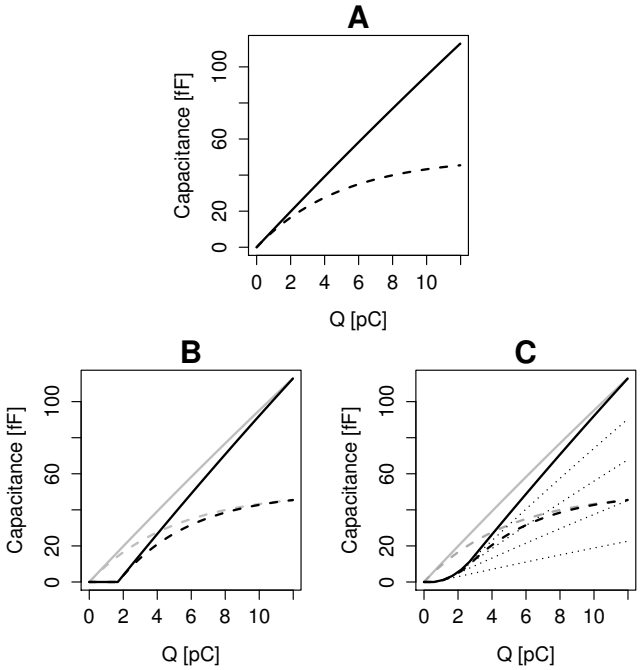

Figure 1:

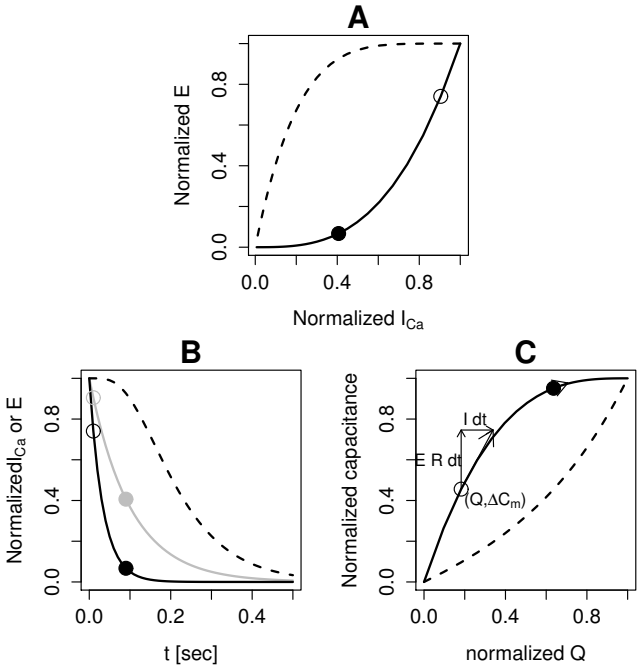
A
Normalized E
0.0
0.4
0.8
0.0
0.4
0.8
Normalized I_{Ca}
B
NormalizedI_{Ca} or E
0.0
0.4
0.8
0.0
0.2
0.4
t [sec]
C
Normalized capacitance
0.0
0.4
0.8
I dt
E R dt
$(Q,\Delta C_m)$
0.0
0.4
0.8
normalized Q

Figure 2:

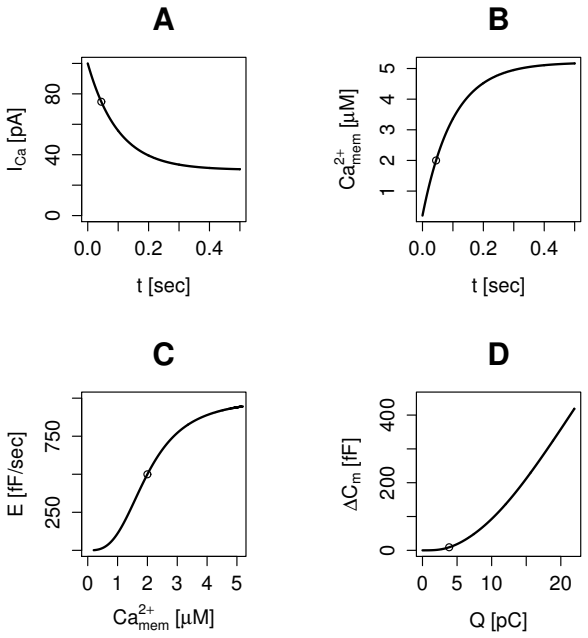
A
B
C
D
I_{Ca} [pA]
0
40
80
0.0
0.2
0.4
t [sec]
Ca^{2+}_{mem} [µM]
1
2
3
4
5
E [fF/sec]
250
750
0
1
2
3
4
5
Ca^{2+}_{mem} [µM]
ΔC_m [fF]
0
200
400
0
5
10
20
Q [pC]

Figure 3:

On depolarization-evoked exocytosis as a function of calcium entry: possibilities and pitfalls
Supporting Material

Morten Gram Pedersen
Lund University Diabetes Centre,
Department of Clinical Sciences,
Lund University, Sweden

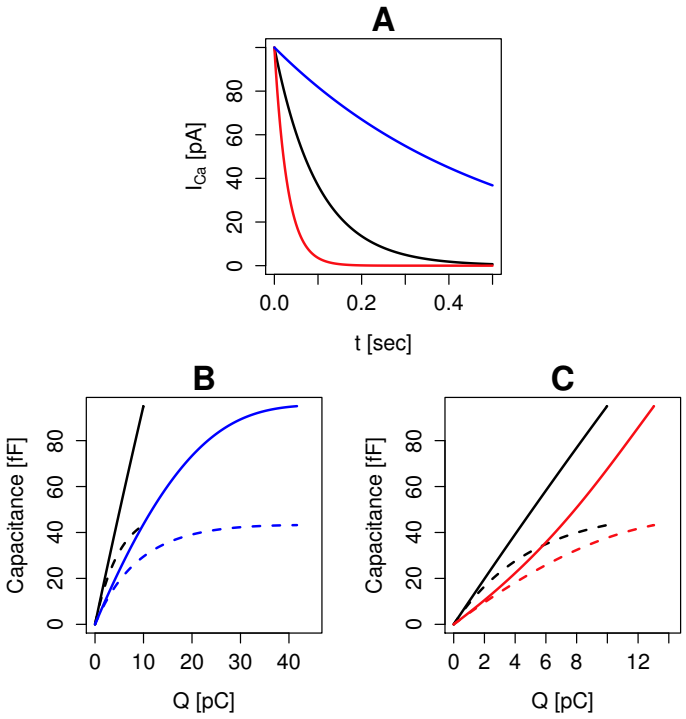

Figure S1: More channel types can change the relation between ΔC_m and Q. A: Exocytosis is assumed to be controlled from nanodomains associated with Ca^{2+}-channels, which inactivate exponentially with a time-constant of 100 ms (black curve, $I_{exo} = 100\,\mathrm{pA}\exp\{-t/100\mathrm{ms}\}$). In addition, the presence of another Ca^{2+}-current type is assumed, either with an inactivation time-constant of 500 ms (blue curve, $I_{slow} = 100\,\mathrm{pA}\exp\{-t/500\mathrm{ms}\}$) or of 30 ms (red curve, $I_{fast} = 100\,\mathrm{pA}\exp\{-t/30\mathrm{ms}\}$). B: The presence of a slowly inactivating Ca^{2+}-current unassociated with exocytosis (panel A, blue curve) accentuates the saturating (exponential, cf. Fig. 1A; black, dashed curve) relation between ΔC_m and Q (blue, dashed curve), while the otherwise linear relation in the absence of pool depletion (cf. Fig. 1A; black, solid curve) becomes concave (blue, solid curve). C: The relation between ΔC_m and Q is changed from exponential (with pool depletion; black, dashed curve) or linear (no pool depletion; black, solid curve) to sigmoidal (with pool depletion; red, dashed curve) or convex (no pool depletion; red, solid curve) in the presence of a rapidly inactivating Ca^{2+}-current unassociated with exocytosis (panel A, red curve). ΔC_m was calculated from I_{exo} as in Fig. 1A, whereas $Q = \int_0^t (I_{exo} + I_{slow})dt$ (panel B) or $Q = \int_0^t (I_{exo} + I_{fast})dt$ (panel C).

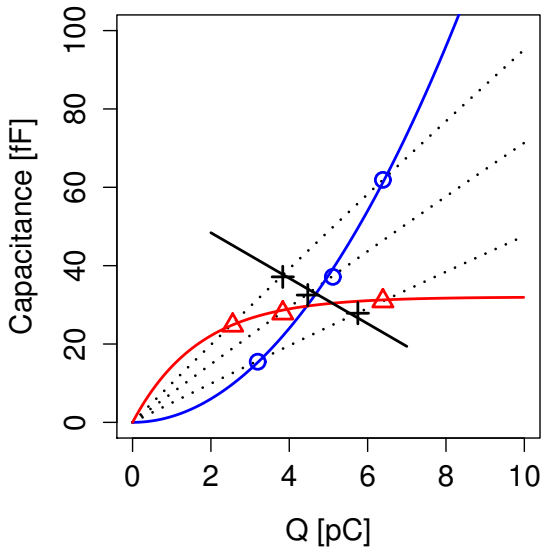

Figure S2: Varying $[Ca^{2+}]_e$ or pulse potential. The black, dotted lines reflect the linear relation (no pool depletion) from Eq. 7 as in Fig. 1A, but for three different values of $A = 0.01/\text{pC}$, $0.0075/\text{pC}$ or $0.005/\text{pC}$ (upper to lower line). If Q and A both increase or decrease when $[Ca^{2+}]_e$ or the pulse potential is varied, then a convex relation between ΔC_m and Q arises (blue circles and curve, $\Delta C_m = 1.5\,Q^2$), while a concave (red triangles and curve, $\Delta C_m = 32[1-\exp(-Q/1.7)]$) or a decreasing (black crosses and curve, $\Delta C_m = 60 - 5.8\,Q$) can be obtained when Q and A are inversely related.

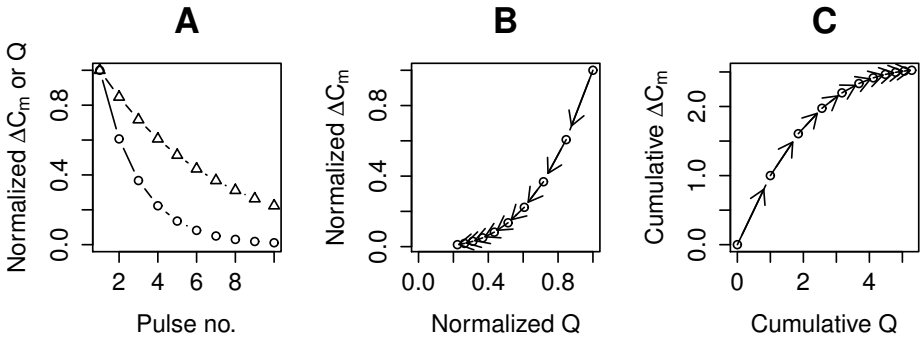

Figure S3: Train protocol. A: Under, for example, the assumption of pool depletion, ΔC_m (circles) declines faster than Q (triangles) from pulse to pulse. B: Plotting ΔC_m versus Q per pulse yields a convex relationship. The curve is followed from high to low values (south-west direction). C: Plotting cumulative ΔC_m versus cumulative Q yields in contrast a concave relationship. The curve is followed from low to high values (north-east direction).